

# D-Flow: A Real Time Spatial Temporal Model for Target Area Segmentation

Wentao Lu, Claude Sammut

School of Computer Science and Engineering  
The University of New South Wales  
{wentao.lu, c.sammut}@unsw.edu.au

## Abstract

Semantic segmentation has attracted a large amount of attention in recent years. In robotics, segmentation can be used to identify a region of interest, or *target area*. For example, in the RoboCup Standard Platform League (SPL), segmentation separates the soccer field from the background and from players on the field. For satellite or vehicle applications, it is often necessary to find certain regions such as roads, bodies of water or kinds of terrain. In this paper, we propose a novel approach to real-time target area segmentation based on a newly designed spatial temporal network. The method operates under domain constraints defined by both the robot's hardware and its operating environment. The proposed network is able to run in real-time, working within the constraints of limited run time and computing power. This work is compared against other real time segmentation methods on a dataset generated by a Nao V6 humanoid robot simulating the RoboCup SPL competition. In this case, the target area is defined as the artificial grass field. The method is also tested on a maritime dataset collected by a moving vessel, where the aim is to separate the ocean region from the rest of the image. This dataset demonstrates that the proposed model can generalise to a variety of vision problems.

**Keywords**— Robot Vision, Spatial-Temporal Learning, Semantic Segmentation

## Introduction

The aim of the work presented here is to efficiently segment regions of interest in a robot's vision system. Image segmentation must work within a set of tight constraints. The computational resources available on-board a robot are often very limited. Furthermore, conserving power is critical in mobile robot, which often leads to trade-offs in computing power, making running time a major concern. Dynamic lighting conditions significantly affect the robot's vision, hence many colour-based vision segmentation methods fail.

There have been many recent proposals for real time image segmentation. However, most of them focus on static semantic segmentation and cannot function effectively under the above constraints. Because of the focus on static images, they do not take advantage of temporal information in a video stream.

Assuming that robot vision can be treated as processing a sequence of images, the model proposed in this paper tries to learn from both spatial and temporal information based on a number of

consecutive frames to predict the segmentation of region of interest (ROI) of the final frame. Figure 1 presents a structural overview of the proposed model, called *D-Flow* because it has two spatial temporal sub-nets to process the data flow in two colour spaces. The basic recurrent unit is a newly designed cell where we introduce convolution operations into a simplified gated recurrent unit known as the Minimal Gated Unit (Zhou et al. 2016). This new convolutional recurrent cell can perform spatial temporal feature extraction while significantly reducing the number of parameters involved.

There are two main reasons for splitting the data flow into two separate sub-nets. First, the model should be robust to changing lighting conditions. Second, although the transform from RGB to YUV is linear and it can be done with a single flow, a single flow architecture can result in a larger number of parameters. Splitting the data into two flows acts as a heuristic to guide each flow to emphasise a particular sub task, which we describe below.

In our first experiment, the SPL robot vision dataset is obtained from a Nao V6 humanoid robot<sup>1</sup> and the ROI or *target area* is defined as the soccer field as per the rules of the RoboCup SPL competition. Our model and two other real time semantic segmentation methods, Fast-SCNN (Poudel, Liwicki, and Cipolla 2019) and a Fully Convolutional Segmentation Network (Long, Shelhamer, and Darrell 2015), are trained on this dataset for comparison. The results are analysed, both quantitatively and qualitatively.

The rest of this paper is organised as follows: first, we address related work, discussing other spatial temporal models and semantic segmentation methods. The design of the new model is described in the following section. We then compare both the quantitative and qualitative results from the SPL dataset with the other two baseline models along with another handcrafted methods. Also, we apply the proposed model to a Maritime dataset to demonstrate the generality of the method. We also perform a set of experiments with different colour spaces to explain why YUV and RGB are chosen in our model.

## Related work

The two main components of this work are the Spatial Temporal Learning model and the Vision Segmentation method. In this section, we discuss previous work related to these two components.

## Spatial Temporal Learning Model

Spatial Temporal Learning models are capable of learning both spatial and temporal information based on a dataset. One method for combining Spatial and Temporal Learning models is the introduction of both a convolution network (LeCun et al. 1999) and a

<sup>1</sup><https://www.softbankrobotics.com/emea/en/nao>

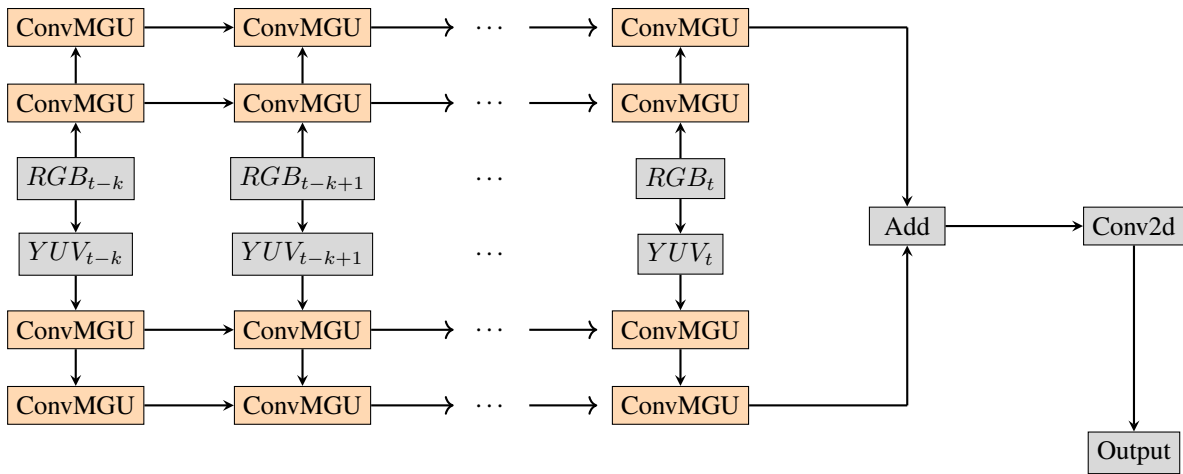


Figure 1: D-Flow Network Overview

recurrent network into a single model. Previous work has presented different alternatives to doing this. Donahue *et al.* (Donahue et al. 2015) proposed a combined model where the image data are fed into the CNN layers first to extract visual features that are then processed by a sequence of LSTM (Gers, Schmidhuber, and Cummins 2000)(Hochreiter and Schmidhuber 1997) units to encode temporal features. This is shown in Figure 2.

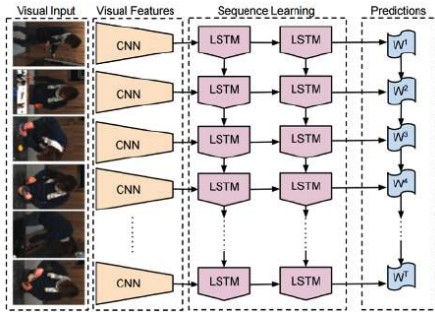


Figure 2: Long-term Recurrent Convolution Networks

Another similar approach was proposed by Tran *et al.* (Tran et al. 2015). The authors describe a 3D convolutional neural network, shown in Figure 3, where the third dimension of each convolution kernel is a convolution operation over time. This model does not contain any recurrent units that require previous states as an extra input to the process. Therefore, one of the major advantages of this model is that its run time is faster than those models based on recurrent networks.

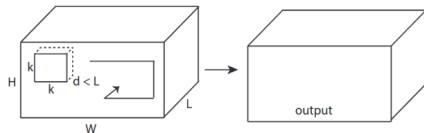


Figure 3: 3D-Convolutional Neural Networks

Figure 4 shows a novel convolutional recurrent unit along with an encoder-decoder structure proposed by Shi et al. (SHI et al.

2015), much like the cascade architecture introduced by Donahue *et al.* The main innovation of this model is that the authors have replaced the internal matrix multiplication operation with a convolution operation that allows spatial features to be extracted by the new recurrent unit. While the model is successful in solving certain problems, there is a drawback when applying it to real-time robotics problems, which is the relatively complex cell structure and large number of parameters, since the base model is a LSTM.

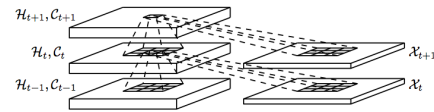


Figure 4: ConvLSTM

## Image Segmentation

There are many recent models capable of performing image segmentation, including FCN (Long, Shelhamer, and Darrell 2015), SegNet (Badrinarayanan, Kendall, and Cipolla 2015) and DeepLabv3+ (Chen et al. 2018). They use an object recognition network, usually a deep CNN structure, as the visual feature encoder followed by a decoder network. These models demonstrate state of the art performance on some image datasets, like COCO(Lin et al. 2015) or PASCAL(Everingham et al. 2010). However, in our case, the only semantic class in our data is a region of interest, which may have an arbitrary shape, depending on the robot's view pose. In other words, the target is not a group of objects but a group of pixels that have similar colours. Furthermore, these object recognition networks usually have a large number of parameters and very complex structures, making them computationally expensive to run in real time on limited hardware.

## Network Structure

In this section, we present a new convolutional recurrent unit, called ConvMGU, and explain the design of both the unit and the D-Flow Network that utilises it.

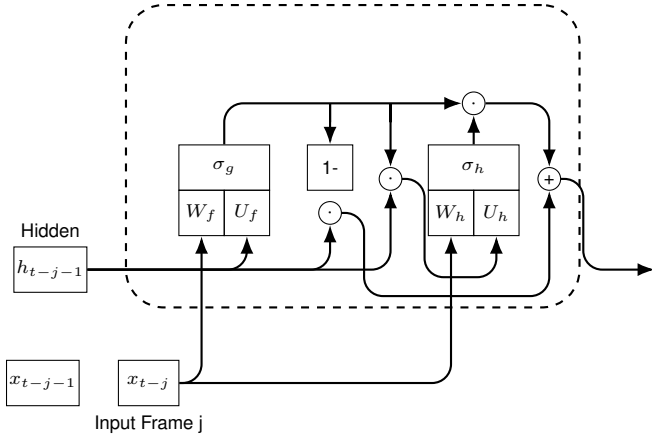


Figure 5: ConvMGU Unit

### Convolutional Minimal Gated Unit

Inspired by the MGU (Zhou et al. 2016) where the authors merge two gates in the original LSTM design to reduce the number of parameters, we borrow this idea to solve a similar problem when designing the new convolution recurrent unit. Figure 5 shows the infrastructure of this unit.

$$f_t = \sigma_g(W_f * x_t + U_f * h_{t-1} + b_f) \quad (1)$$

$$h_t = (1 - f_t) \circ h_{t-1} + f_t \circ \sigma_h(W_h * x_t + U_h * (f_t \circ h_{t-1}) + b_h) \quad (2)$$

Equations 1 and 2 are modified from the original MGU paper where the internal matrix multiplications are replaced with convolution operations as denoted by  $*$ .  $f_t$  is the output of the current step. It is used, along with the hidden state  $h_{t-1}$ , coming from the last step, to calculate the hidden state  $h_t$  of the current step. These modifications introduce the ability to extract spatial features while maintaining the major advantage of the original MGU which is the relatively small number of parameters.

One further modification is shown in Figure 6. It stacks two layers of ConvMGU and adds a shortcut later to form a ConvMGU block whose structure is reminiscent of a standard Residual Block (He et al. 2016).

The method proposed by Elsayed *et al* (Elsayed, Maida, and Bayoumi 2018) is used to estimate the number of parameters of the two layer ConvMGU stack, ConvMGU Block and ConvLSTM stack as detailed in Equations 3-5.

$$2 \text{ Layer ConvLSTM} : 2 \times 4 \times (m^2(\gamma + \kappa) + 1) \cdot n \quad (3)$$

$$\text{Our Block} : 2 \times (m^2(\gamma + \kappa) + 1) \cdot n + (f^3 \cdot \gamma + 1) \cdot n \quad (4)$$

$$\text{Our 2 Layer ConvMGU} : 2 \times (m^2(\gamma + \kappa) + 1) \cdot n \quad (5)$$

For the purpose of analysis, the assigned values for each hyperparameter is shown in Table 1.

The results demonstrate that the number of parameters of the proposed ConvMGU block is 73% smaller in comparison with the original two layer ConvLSTM unit.

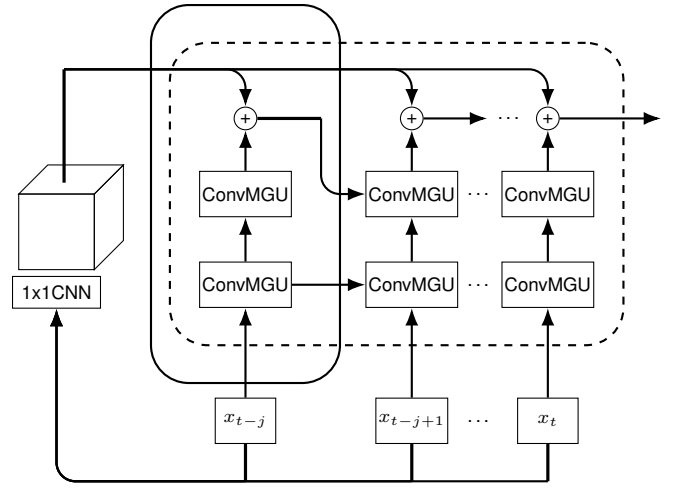


Figure 6: ConvMGU Block

	Meaning	Assigned Value
<b>m</b>	conv kernel size	3
$\gamma$	input channel	3
$\kappa$	number of feature maps	40
<b>n</b>	output channel	40
<b>f</b>	3d conv kernel size	3

Table 1: Unit Setting

### D-Flow Network

The D-Flow Network is composed of two flows of ConvMGU units that encode spatial temporal features derived from input vision frames. The following convolution layer acts as a simple decoder to perform a one-step prediction of the target area segmentation.

As mentioned previously, handling dynamic lighting conditions is a major problems for mobile robots. The appearance of a colour can vary dramatically when the robot operates in natural lighting conditions. This significantly affects target area segmentation, where the target is defined as a group of pixels that have similar colours. To overcome this problem efficiently, the proposed two-flow network takes both YUV and RGB images as input to efficiently search for the best weights. Figure 1 illustrates the proposed network.

The whole network performs a single-step prediction that takes a sequence of input frames and attempts to predict the segmentation of the current frame. The YUV and RGB images are processed separately by stacks of ConvMGU to extract various spatial temporal features. These features are then added together to produce the final feature maps that the subsequent decoder can use for prediction.

### Experiment

In this section we describe a set experiments to analyse the performance and generalisation ability of our model.

#### SPL Vision Dataset

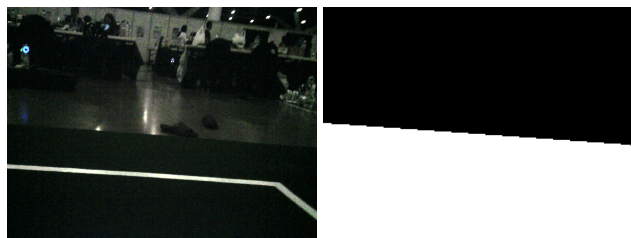
For the first experiment, we used a dataset collected from a Nao V5/V6 humanoid robot from Softbank Robotics(Lu 2021). The dataset contains 20 video captures where each video contains varying numbers of image sequences with corresponding weak labels. The details of the labelled data are shown in the Table 2. The raw

resolution is 1280 by 960. The data were collected from various locations and with different lighting conditions.

#frame	location	lighting condition	body motion	recording type
19	Indoor(Germany)	Constant(low)	Static	Multi-testing
19	Indoor(Germany)	Constant(low)	Static	Multi-testing
19	Indoor(Germany)	Constant(low)	Static	Multi-testing
5	Indoor(Germany)	Constant(high)	Static	Single-testing
6	Indoor(Germany)	Constant(high)	Static	Single-testing
19	Indoor(Germany)	Constant(low)	Dynamic	Single-testing
7	Indoor(Germany)	Constant(low)	Dynamic	Game
259	Indoor(UNSW)	Constant(medium)	Dynamic	Single-testing
199	Outdoor(Sydney)	Night	Static	Single-testing
121	Indoor(UNSW)	Uneven(medium)	Dynamic	Single-testing
271	Indoor(UNSW)	Uneven(medium)	Dynamic	Multi-testing
113	Indoor(UNSW)	Uneven(medium)	Dynamic	Multi-testing
68	Outdoor(Sydney)	Night	Static	Single-testing
119	Outdoor(Sydney)	Night	Static	Single-testing
298	Indoor(Sydney)	Constant(low)	Dynamic	Multi-testing
251	Outdoor(Sydney)	Morning(uneven)	Static	Single-testing
210	Indoor(UNSW)	Extremely uneven	Dynamic	Single-testing
181	Indoor(UNSW)	Extremely uneven	Dynamic	Single-testing
213	Indoor(UNSW)	Extremely uneven	Dynamic	Multi-testing
188	Indoor(UNSW)	Extremely uneven	Dynamic	Multi-testing

Table 2: Dataset Information

Figure 7 presents a pair of raw images and a label that is used to identify noisy target areas using white shapes. A labelling tool is used to manually mark and generate the white shape that is considered to be the labelled target area. The goal for this dataset is to train a model that can identify these target areas with minimal false positives under dynamic lighting conditions. We hypothesise that such a model may even be able to overcome issues introduced by the weak labelling. Since it is a weak labelling system, the lines and all other objects present within the target area are all given the same label.



(a) Raw Image

(b) Label

Figure 7: A sample pair of SPL dataset

## Experiment Results

In this experiment we performed target area segmentation with Fast-SCNN, a Fully Convolution Network and our model. Input images were down-sampled four times to 320 by 240 for efficiency. All training was performed on a single NVIDIA RTX 1060 and the inference time analyses were done on the same GPU. The experiment was implemented using the Pytorch 1.7.1 (Paszke et al. 2017).

Figures 8 and 9 present the qualitative results for two test sequences generated by the candidate methods with different loss functions. The third set of results was generated by our model with Focal Loss (Lin et al. 2017) while the others were trained with Binary Cross Entropy Loss.

As the images show, the FCN only learned positional patterns and failed to generalise properly in different scenarios. Fast-SCNN learnt some out-of-domain patterns, as it showed the ability to generalise through its identification of the green area from the bottom

part of the images. Unfortunately, it tended to overfit based on the colour pattern since it labelled all the green parts as the target area even though some of them were simple light reflections. The left-most three images demonstrate the ability of our model to outperform the other models in this task. All of them label most parts of the target area with minimal outliers that can be easily removed through post-processing. However, only our models were able to crop out random objects in the target area. This demonstrates that our model can work effectively with a weak labelling system which has noisy labels.

For a quantitative analysis, we used two different metrics to measure segmentation performance. The Dice Coefficient (Dice 1945) is a statistic that measures the similarity between two samples that we use in this experiment to measure the model’s ability to learn label patterns. This score only measures how well the model fits the labels, where the labels may be noisy. Therefore, it does not measure the true ability for target area segmentation but acts as a base check for learning outcomes. The silhouette score (Rousseeuw 1987) is another metric that is a model-free measurement of the consistency in segmentation. The inference time analysis shown was performed on a single NVIDIA RTX 1060 GPU. The results are shown in Table 3.

	Dice Score	Silhouette score	Inference Time	#Params
<b>Ours_small</b>	0.82	26%	19 ms	<b>45K</b>
<b>Ours</b>	0.83	<b>27%</b>	41 ms	0.178M
<b>FCN(VGG)</b>	0.85	24%	31 ms	32M
<b>Fast-SCNN</b>	<b>0.91</b>	26%	<b>12ms</b>	1.1M

Table 3: Quantitative Results

## Comparison with Handcrafted Methods

In this section, we compare the proposed model with two handcrafted methods used by the RoboCup team, rUNSWift, where both of them perform field recognition (Brameld et al. 2018).

Adaptive-thresholding is an algorithm that groups pixels into binary classes in a sliding window. As shown in Figures 10 and 11, two variants are actually doing brightness-based clustering which is suitable for finding certain objects. Unfortunately, these methods are not able to tell the difference between the main part of the soccer field and the image background, where in most cases, they are both shown as a darker colour.

A distance-transform is one step in the Watershed background extraction(Roerdink and Meijster 2000). Since its purpose is to distinguish between the foreground and background, it is not suitable for use in target area segmentation. As shown, it marks white clusters inside the soccer field as well as random bright pixels as foreground. Therefore, its output is a mixture of a part of the target area and a part of the darker background.

## Experiments on Maritime Dataset

We tested our work on a maritime dataset to see how well the proposed method performs in different domains. The Singapore Maritime Dataset(SMD) (Prasad et al. 2017) was used in this experiment. It contains two different subsets. In our experiment, we only used the one where the camera is mounted on a moving vessel, which is similar to a mobile robot.

Dataset	Sub-set	#Video	#Frames/Video	#Total
SMD	On-Board	11	300	3300

Table 4: SMD dataset



Figure 8: Comparison Experiment Result 1

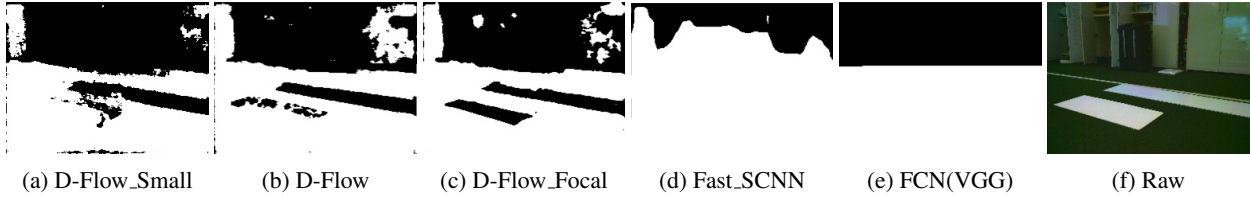


Figure 9: Comparison Experiment Result 2

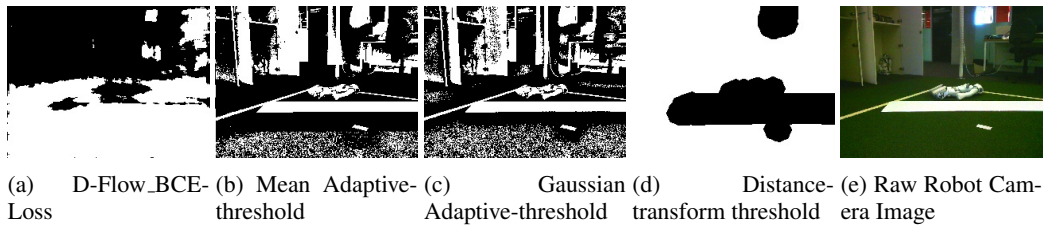


Figure 10: Experiment comparing against Handcrafted Methods Result 1

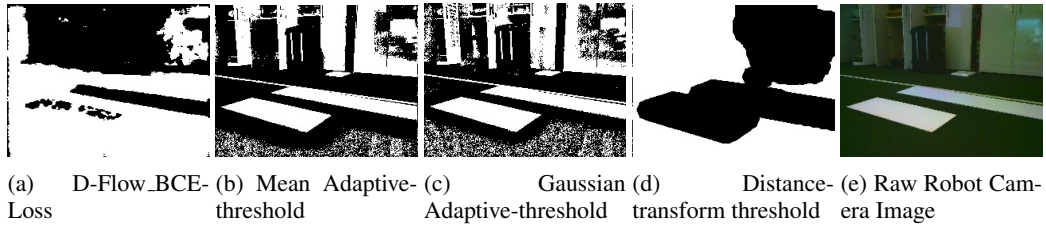


Figure 11: Experiment comparing against Handcrafted Methods Result 2

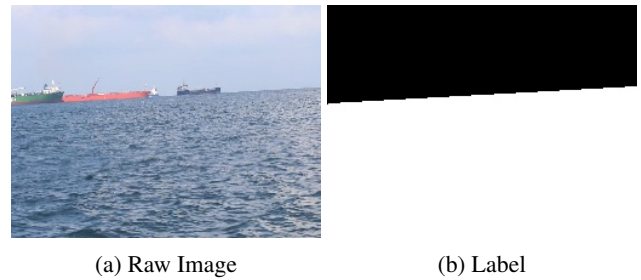
Table 4 gives the details of the subset of the data we used in this test. We used 9 of the 11 videos as training data and the remaining 2 as test data. In this task, we defined the target area as the ocean below horizon. Figure 12 shows a pair of sample raw frames and the corresponding label. Again, we used a weak labelling system as we only put a rectangular mask as the target.

Figure 13 shows a sample output for the test data. We can see that despite the big difference in the ocean colour between the test data and the sample training data, our model can still find the target region of the ocean below the horizon with not many false positives.

### Experiment with Different Colour Spaces

Our model is composed of two sub-nets that process RGB and YUV formatted data separately until the processed feature maps are combined for the final prediction stage.

We conducted a series of experiments with the SMD dataset to understand the effects of using different colour spaces and the network architecture. Table 5 in Appendix shows the setting for each



(a) Raw Image (b) Label

Figure 12: a sample pair of SMD dataset

experiment.

Figure 14 in the Appendix shows the learning curves for each experiment. We see the RGB-YUV combination with the Double-Flow architecture achieves the most stable performance and lowest validation loss at the 100th epoch. The YUV-only model suffers

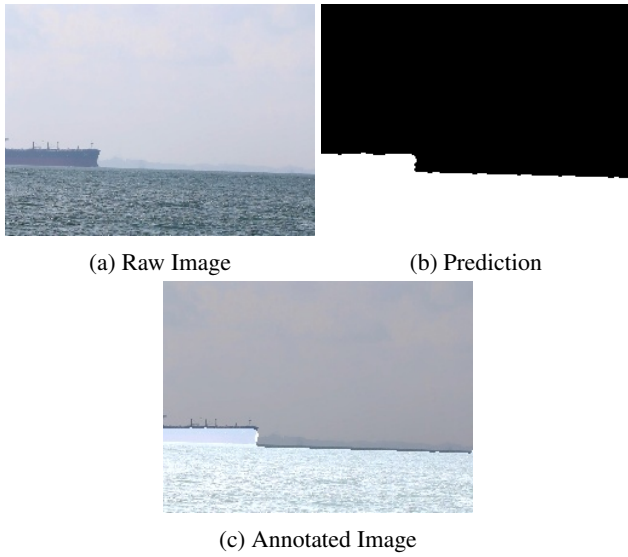


Figure 13: Sample output for SMD dataset

from underfitting while HSV-only and the HSV-YUV combination suffer from overfitting. The RGB-YUV(Y-Only) experiment is intended to determine if the gray scale image has the same effect as a full YUV image. The RGB-YUV(Y-Only) can achieve low validation loss at some epochs, but the learning curve is quite unstable and tends to fluctuate dramatically while achieving low validation loss. In conclusion, among all these different colour space settings and network architectures, the RGB-YUV combination with Double-Flow net is the best.

### Conclusion

We have proposed a new approach to real time robot vision target area segmentation along with a new parameter reduced convolutional recurrent unit. The proposed D-Flow Network demonstrates the ability to overcome problems including dynamic lighting conditions. We have also created and published a robot vision dataset that was obtained using a Nao V5/V6 robot. This dataset can be used for a variety of robot vision problems.

## Appendices

### Learning Curves for Different Colour Space

Models	Colour for 1st flow	Colour for 2nd flow
Single-Flow	RGB	N/A
Single-Flow	HSV	N/A
Single-Flow	YUV	N/A
Double-Flow	RGB	YUV
Double-Flow	RGB	HSV
Double-Flow	HSV	YUV
Double-Flow	RGB	YUV(Y-Only)

Table 5: Experiment Settings

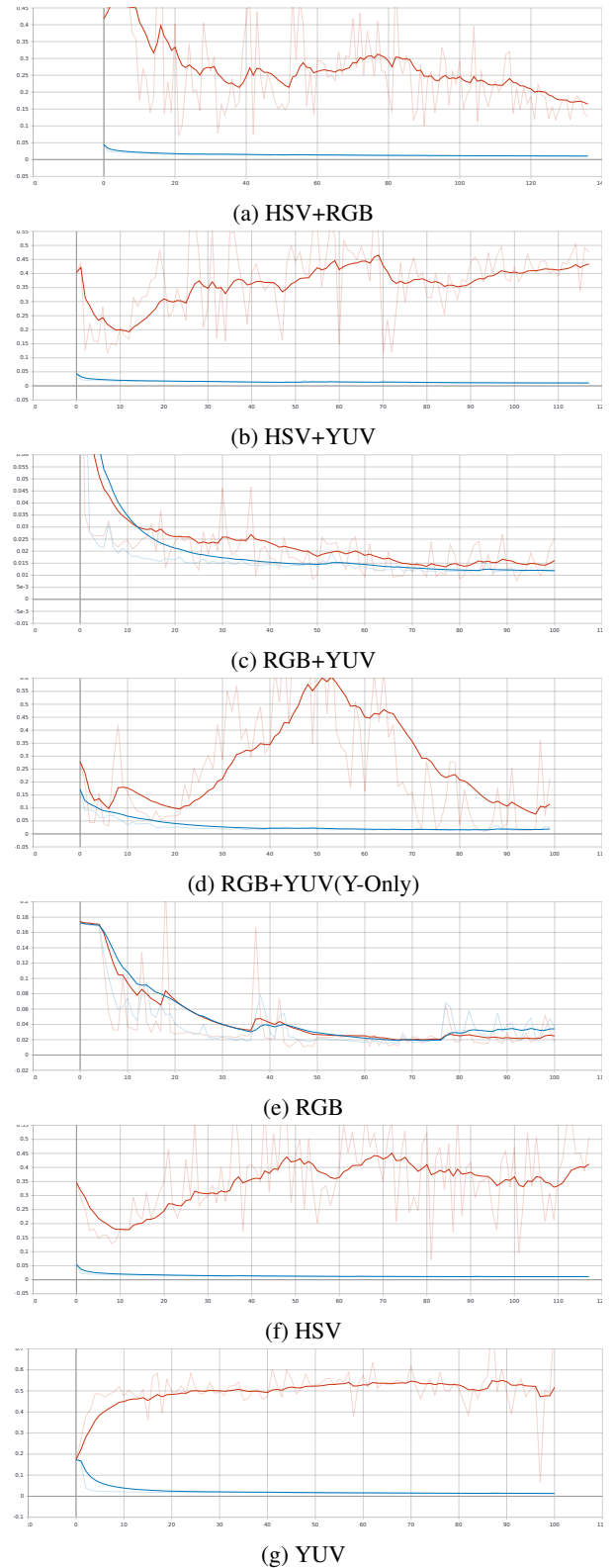


Figure 14: Learning Curves

## References

- Badrinarayanan, V.; Kendall, A.; and Cipolla, R. 2015. SegNet: A Deep Convolutional Encoder-Decoder Architecture for Image Segmentation. *CoRR*, abs/1511.00561.
- Brameld, K.; Hamersley, F.; Jones, E.; Kaur, T.; Li, L.; Lu, W.; Pagnucco, M.; Sammut, C.; Sheh, Q.; Schmidt, P.; et al. 2018. RoboCup SPL 2018 rUNSWift Team Paper.
- Chen, L.-C.; Zhu, Y.; Papandreou, G.; Schroff, F.; and Adam, H. 2018. Encoder-Decoder with Atrous Separable Convolution for Semantic Image Segmentation. In *The European Conference on Computer Vision (ECCV)*.
- Dice, L. R. 1945. Measures of the Amount of Ecologic Association Between Species. *Ecology*, 26(3): 297–302.
- Donahue, J.; Anne Hendricks, L.; Guadarrama, S.; Rohrbach, M.; Venugopalan, S.; Saenko, K.; and Darrell, T. 2015. Long-Term Recurrent Convolutional Networks for Visual Recognition and Description. In *The IEEE Conference on Computer Vision and Pattern Recognition (CVPR)*.
- Elsayed, N.; Maida, A. S.; and Bayoumi, M. 2018. Reduced-Gate Convolutional LSTM Using Predictive Coding for Spatiotemporal Prediction. *CoRR*, abs/1810.07251.
- Everingham, M.; Van Gool, L.; Williams, C. K. I.; Winn, J.; and Zisserman, A. 2010. The Pascal Visual Object Classes (VOC) Challenge. *International Journal of Computer Vision*, 88(2): 303–338.
- Gers, F. A.; Schmidhuber, J.; and Cummins, F. 2000. Learning to Forget: Continual Prediction with LSTM. *Neural Computation*, 12(10): 2451–2471.
- He, K.; Zhang, X.; Ren, S.; and Sun, J. 2016. Deep Residual Learning for Image Recognition. In *The IEEE Conference on Computer Vision and Pattern Recognition (CVPR)*.
- Hochreiter, S.; and Schmidhuber, J. 1997. Long Short-Term Memory. *Neural Computation*, 9(8): 1735–1780.
- LeCun, Y.; Haffner, P.; Bottou, L.; and Bengio, Y. 1999. *Object Recognition with Gradient-Based Learning*, 319–345. Berlin, Heidelberg: Springer Berlin Heidelberg. ISBN 978-3-540-46805-9.
- Lin, T.-Y.; Goyal, P.; Girshick, R.; He, K.; and Dollár, P. 2017. Focal loss for dense object detection. In *Proceedings of the IEEE international conference on computer vision*, 2980–2988.
- Lin, T.-Y.; Maire, M.; Belongie, S.; Bourdev, L.; Girshick, R.; Hays, J.; Perona, P.; Ramanan, D.; Zitnick, C. L.; and Dollár, P. 2015. Microsoft COCO: Common Objects in Context. arXiv:1405.0312.
- Long, J.; Shelhamer, E.; and Darrell, T. 2015. Fully Convolutional Networks for Semantic Segmentation. In *The IEEE Conference on Computer Vision and Pattern Recognition (CVPR)*.
- Lu, W. 2021. The rUNSWift SPL Field Segmentation Dataset. arXiv:2108.12809.
- Paszke, A.; Gross, S.; Chintala, S.; Chanan, G.; Yang, E.; DeVito, Z.; Lin, Z.; Desmaison, A.; Antiga, L.; and Lerer, A. 2017. Automatic Differentiation in PyTorch. In *NIPS Autodiff Workshop*.
- Poudel, R. P. K.; Liwicki, S.; and Cipolla, R. 2019. Fast-SCNN: Fast Semantic Segmentation Network. *CoRR*, abs/1902.04502.
- Prasad, D. K.; Rajan, D.; Rachmawati, L.; Rajabally, E.; and Quek, C. 2017. Video Processing From Electro-Optical Sensors for Object Detection and Tracking in a Maritime Environment: A Survey. *IEEE Transactions on Intelligent Transportation Systems*, 18(8): 1993–2016.
- Roerdink, J. B.; and Meijster, A. 2000. The watershed transform: Definitions, algorithms and parallelization strategies. *Fundamenta informaticae*, 41(1, 2): 187–228.
- Rousseeuw, P. J. 1987. Silhouettes: A graphical aid to the interpretation and validation of cluster analysis. *Journal of Computational and Applied Mathematics*, 20: 53 – 65.
- SHI, X.; Chen, Z.; Wang, H.; Yeung, D.-Y.; Wong, W.-k.; and WOO, W.-c. 2015. Convolutional LSTM Network: A Machine Learning Approach for Precipitation Nowcasting. In Cortes, C.; Lawrence, N. D.; Lee, D. D.; Sugiyama, M.; and Garnett, R., eds., *Advances in Neural Information Processing Systems 28*, 802–810. Curran Associates, Inc.
- Tran, D.; Bourdev, L.; Fergus, R.; Torresani, L.; and Paluri, M. 2015. Learning Spatiotemporal Features With 3D Convolutional Networks. In *The IEEE International Conference on Computer Vision (ICCV)*.
- Zhou, G.-B.; Wu, J.; Zhang, C.-L.; and Zhou, Z.-H. 2016. Minimal gated unit for recurrent neural networks. *International Journal of Automation and Computing*, 13(3): 226–234.